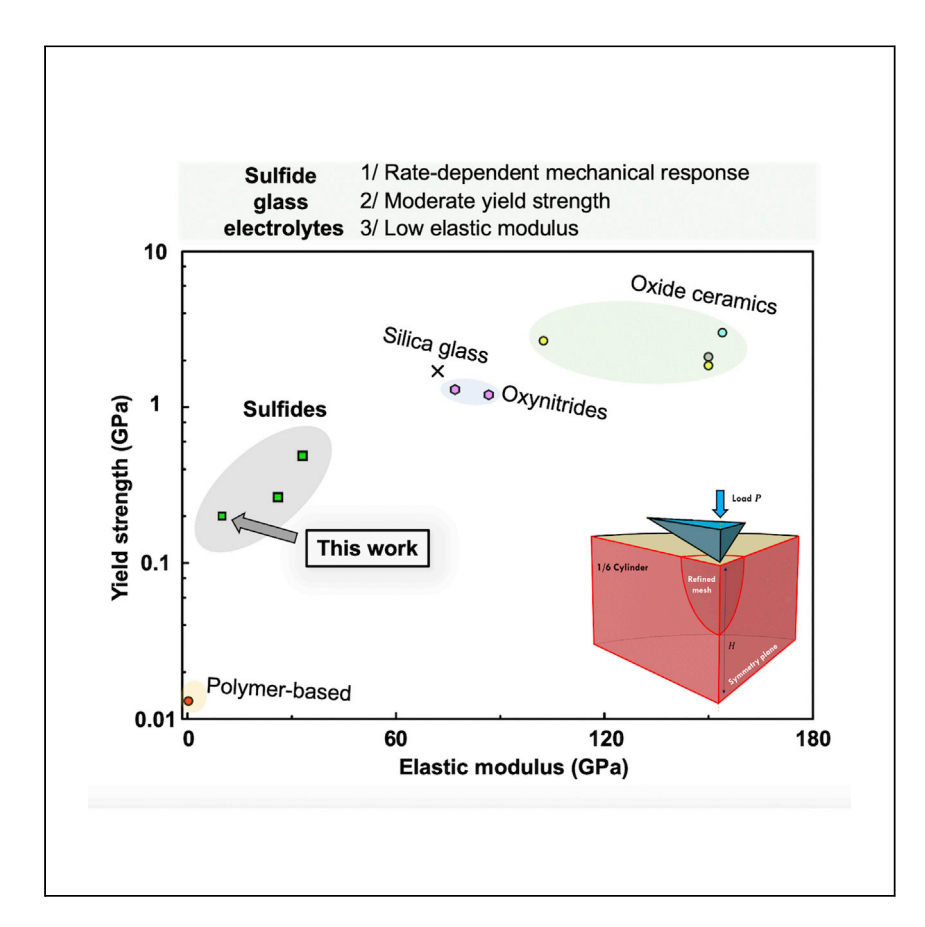


Article

Rate-dependent deformation of amorphous sulfide glass electrolytes for solid-state batteries



Athanasiou et al. investigate the mechanical behavior of sulfide glass electrolytes and demonstrate that the deformation of these materials differs substantially from that of other solid electrolytes. The observed rate-dependent deformation of sulfide electrolytes is expected to have a significant impact on battery performance.

Christos E. Athanasiou, Xing Liu, Mok Yun Jin, ..., Nitin P. Padture, Huajian Gao, Brian W. Sheldon

christos_edouardos_athanasiou@brown. edu (C.E.A.)

brian_sheldon@brown.edu (B.W.S.)

Highlights

Amorphous sulfide electrolytes exhibit viscoplastic mechanical behavior

An integrated material characterization framework is developed

Viscoplasticity in the electrolytes is important in lithium metal penetration of sulfide glasses

Athanasiou et al., Cell Reports Physical Science 3, 100845

April 20, 2022 © 2022 The Authors. https://doi.org/10.1016/j.xcrp.2022.100845





Article

Rate-dependent deformation of amorphous sulfide glass electrolytes for solid-state batteries

Christos E. Athanasiou, 1,6,7,* Xing Liu, 1,6 Mok Yun Jin, 1 Eugene Nimon, 2 Steve Visco, 2 Cholho Lee, 3 Myounggu Park, 3 Junnyeong Yun, 3 Nitin P. Padture, 1 Huajian Gao, 1,4,5 and Brian W. Sheldon 1,*

SUMMARY

Sulfide glasses are emerging as potential electrolytes for solid-state batteries. The mechanical behavior of these materials can significantly impact cell performance, and it is thus imperative to understand their deformation and fracture mechanisms. Previous work mainly reports properties obtained under quasi-static loading conditions, but very little is known about deformation under dynamic conditions. The current investigation shows that the sulfide glass mechanical behavior is dominated by viscoplasticity, differing substantially from polycrystalline oxide and sulfide solid electrolytes. Finite element modeling indicates that the sulfide glass stiffness is high enough to maintain good contact with softer lithium metal electrodes under moderate stack pressures. The observed viscoplasticity also implies that battery operating conditions will play an important role in electro-chemo-mechanical processes that are associated with dendritic lithium penetration. In general, the rate-dependent mechanical behavior of the sulfide glass electrolytes documented here offers a new dimension for designing next-generation all-solid-state batteries.

INTRODUCTION

Realizing the full potential of lithium-ion batteries (LIBs) in emerging decarbonized applications over the coming decades demands high-performance cell components. Electrolytes that can enable Li-metal electrodes are extremely attractive. These systems can outperform the intercalation-based anodes employed in current LIBs in terms of both gravimetric and volumetric energy densities. One of the most challenging issues in enabling Li-metal electrodes is replacing the liquid ion-conducting electrolyte in the conventional LIB with a solid electrolyte, i.e., creating a solid-state battery (SSB) configuration. 1–5

Most of the SSB electrolytes suffer from low ionic conductivities (less than $\sim \! 10^{-4} \ S \ cm^{-1})$ compared with liquid electrolytes ($\sim \! 10^{-2} \! - \! 10^{-3} \ S \ cm^{-1})$. Sulfide glasses (e.g., Li₂S–P₂S₅) are promising electrolyte materials that can overcome this limitation. $^{6-15}$ Dense materials are typically formed by melt processing, followed by cold pressing. 15 It is known that the mechanical properties of solid electrolytes have an important impact on the cell performance. However, a complete description of the mechanical behavior of sulfide electrolytes has not been reported. Previous studies focus on their mechanical properties under quasi-static loading conditions, rather than their deformation under dynamic loading, which is more relevant to the real battery operating conditions. 15 In this context, systematic characterization is required to understand the mechanical response of the sulfide glasses under various loading rates.



¹School of Engineering, Brown University, Providence, RI 02912, USA

²Polyplus Battery Company, Berkeley, CA 94710, USA

³Institute of Environmental Science & Technology, SK Innovation, Daejeon 34124, Republic of Korea

⁴School of Mechanical and Aerospace Engineering, College of Engineering, Nanyang Technological University, Singapore 639798, Singapore

⁵Institute of High Performance Computing, A*STAR, Singapore 138632, Singapore

⁶These authors contributed equally

⁷Lead contact

^{*}Correspondence:

christos_edouardos_athanasiou@brown.edu (C.E.A.), brian_sheldon@brown.edu (B.W.S.) https://doi.org/10.1016/j.xcrp.2022.100845



The present work reveals that the mechanical behavior of sulfide glass electrolytes is rate dependent and governed by viscoplasticity. Finite element (FEM) simulations informed by indentation experiments provide a quantitative material model that fully describes the viscoplastic deformation of the materials. This model offers a platform for understanding how sulfide glass electrolytes interact with Li-metal anodes during battery operation. It is found that a conformal anode-electrolyte contact can be maintained under moderate stack pressures. Furthermore, model predictions show that viscoplasticity can substantially alter the impact of battery charging rates on Li-metal (dendritic) penetration.

RESULTS AND DISCUSSION

Creep response of the sulfide glass via indentation

The specimens for this investigation (described in experimental procedures) were prepared by melt quenching. They were provided by two different suppliers and are identified here as sample 1 (Umicore) and sample 2 (Materion). Indentation-based methods were used to quantify the fundamental mechanical properties of these amorphous solid electrolytes, including elastic, plastic, and fracture behaviors. ^{16–20} These approaches are advantageous because the reactivity of these materials makes it challenging to employ relevant American Society for Testing and Materials (ASTM) standard tests or sophisticated micro-testing. ^{21–23} In particular, mechanical characterization of these sulfide glass samples is exceptionally challenging due to their extreme moisture sensitivity (exposure to air quickly degrades the sample surfaces). To eliminate contamination, a specialized vacuum can was assembled for transferring and storing the samples (Figure S1). Furthermore, all specimens were immersed in protective mineral oil during indentation tests to suppress possible chemical degradation (more information in experimental procedures).

Instrumented indentation equipped with a (Berkovich) fluid cell tip (Figure 1A) was performed to understand the elastic and plastic responses of the sulfide glass electrolytes. ^{16–19} Figures 1B and 1C show indentation load-displacement curves for the two materials, both of which feature a bow shape in the initial part of the unloading curves. This unloading response is indicative of creep deformation and cannot be used to calculate the hardness and Young's modulus of the sulfide glass materials. ¹⁶

Vickers indentation was performed to investigate the fracture responses of the sulfide glass electrolytes (sample 1). Radial cracks were generated by the impression of an indenter tip in a load-controlled manner, emanating from the edge of the indentation corner (shown in Figure 2). Typically, a loading pattern as shown in Figure 2A is applied. The indenter loading durations were fixed at 30 s while the applied load (9.8, 11.2, 14.0, and 15.0 N, respectively) and holding time were varied. The radial crack length (shown in Figure 2B) exhibits a strong dependence on the indentation holding time (Figure 2C). This phenomenon is indicative of the rate-dependent mechanical behavior of the sulfide glasses. The nonconvergent crack length measurement indicates that the resistance to fracture is rate-dependent. To illustrate this issue, we plot the ratio between the power of crack length, $c^{1.5}$, and the maximum indentation load, P, which is expected to be a constant (after sufficient holding times) according to the classic indentation analysis (Equation 3 in experimental procedures). Significant scatter in $c^{1.5}/P$ is indicative of creep deformation (Figure 2D).

The measurements reported in Figures 1 and 2 were repeated after prolonged exposures in the mineral oil (up to 1 h as shown in Figure S2), and the results did not



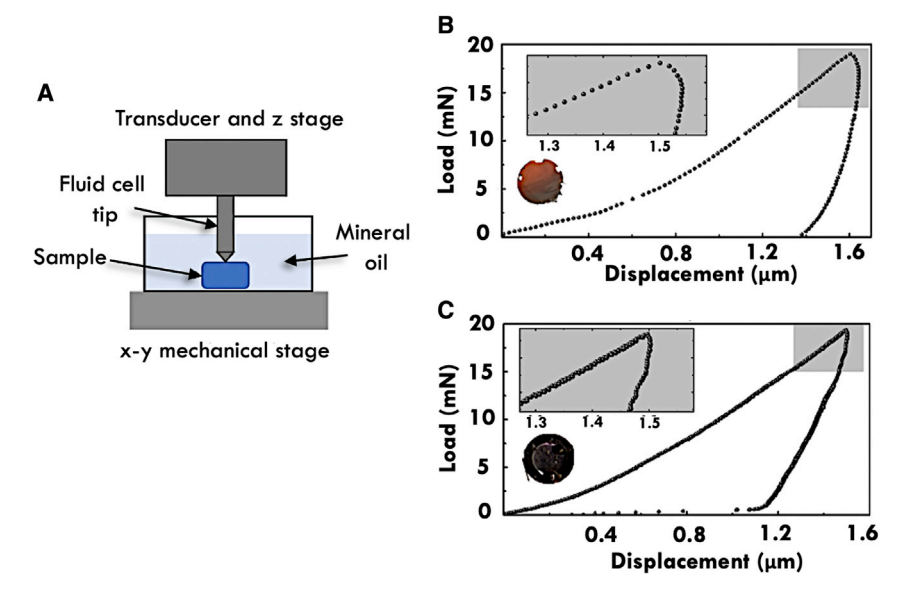


Figure 1. Instrumented indentation in mineral oil for mechanical characterization
(A) The samples were immersed in mineral oil, and a Berkovich fluid cell tip was employed.
(B and C) Samples from two vendors were tested: sample 1 from Umicore and sample 2 from Materion. Their top-view images are shown in the bottom left part of the plots. The indentation load-displacement curves exhibit a bow-shaped unloading segment (magnified in the insets).

vary. This reproducibility confirms that the material is not degrading substantially inside of the mineral oil (despite the presence of trace water in the oil), which is consistent with prior indentation work using similar sulfide glass electrolytes.¹⁵

To characterize the mechanical properties of the sulfide glass electrolytes in a reliable manner, instrumented Berkovich indentation experiments with modified loading patterns were performed. The experimental data were analyzed by FEM simulations. Two main questions are considered in the current investigation: (1) is the rate-dependent behavior of the sulfide glass primarily of viscoelastic or viscoplastic nature? and (2) how do we find an appropriate constitutive model for sulfide glasses?

Simulation-assisted Berkovich indentation

The viscoelastic and viscoplastic effects on the materials response were investigated as shown in Figure 3. A sequence of loading/holding/unloading/holding/unloading with different rates was performed to distinguish the recoverable and non-recoverable deformation (Figures 3A and 3B). More details on this methodology can be found in Yang et al. Figure 3A shows the effect of the loading rate on the first loading segment (identified as a–b in Figure 3B). The overlap of the load-displacement curve for the loading rates of 1.0 mN/s and 2.0 mN/s indicates that both rates are high enough to eliminate undesired viscous effects in the loading step, with the former one being selected for the rest of the experiments. In the following step (b–c in Figure 3B), creep deformation took place while the maximum load was held constant for various durations. The total increase in the nanoindentation displacement during the holding stage was the sum of the viscoelastic and viscoplastic displacements. In the unloading segment (c–d in Figure 3B), all the inviscid elastic deformation was recovered under unloading rate of 1 mN/s. A second holding step for 35 s at less than 5% of the maximum load (d–e in Figure 3B) was performed, during which



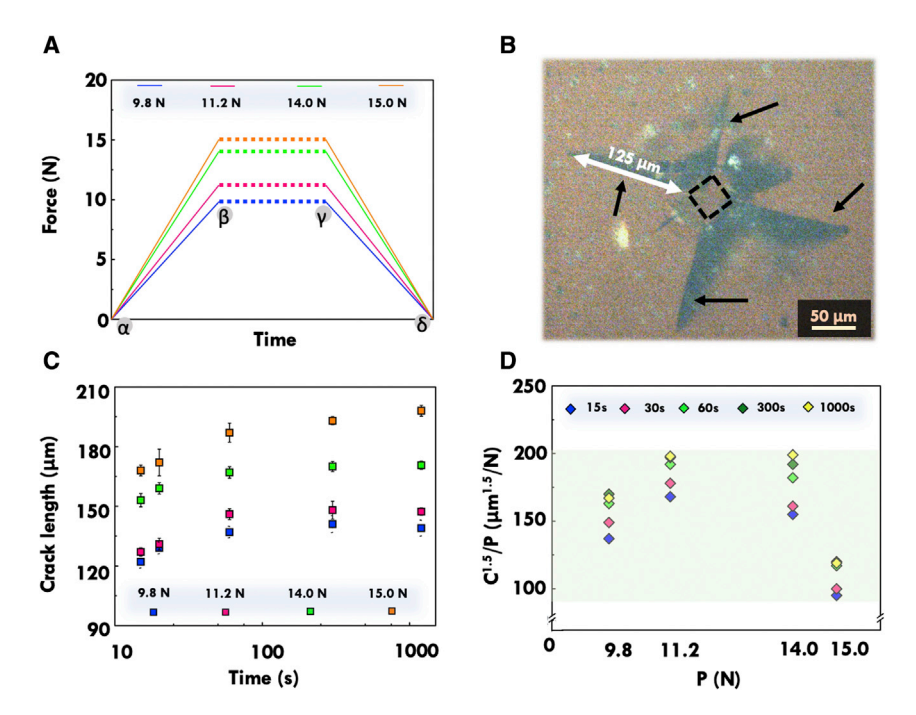


Figure 2. Vickers toughness indentation tests

(A) Loading pattern for the Vickers indentation tests, in which the load and time of the holding step (dashed lines) were varied.

(B) Optical microscopy image (dark field) of sample 1 after indentation-induced cracking. The image corresponds to the indentation test for 9.8 N load and 15 s holding time. The four radial cracks originating from the indenter imprint (dashed squared region) were clearly visible and highlighted by the black arrows. The white double-sided arrow shows the trace of the crack (\sim 125 µm).

(C) Different indentation crack lengths are obtained by varying holding durations and loads. Each data point corresponds to an average of three independent measurements.

(D) The ratio between $c^{1.5}$ (c is crack length) and the maximum indentation load, P, is found to exhibit significant scatter for various loading patterns. This indicates the presence of viscous behavior.

the displacement change was dominated by the recovery of viscoelastic deformation. The comparison of the segments b–c and d–e provides direct evidence of whether the viscous behavior is viscoelastic or viscoplastic in nature. An important observation here is that the deformation during d–e is small compared with that of b–c. This shows that the viscous behavior is governed by viscoplasticity rather than viscoelasticity. Based on the results in Figure 3A, the unloading rate of 1 mN/s in Figure 3C (blue line) is sufficient to suppress the rate dependence, such that the size of the response in d–e does not significantly impact our interpretation.

A phenomenological rate-dependent plasticity model with the Peirce formulation is employed to describe the sulfide glasses. ²⁵ The material constitutive law is based on J_2 flow theory, which features an isotropic rate-dependent yield surface described by

$$\frac{\overline{\sigma}}{Y_{SE}} = \left(1 + \frac{\dot{\overline{\varepsilon}}^{\rho}}{D}\right)^{\frac{1}{n}}$$
 (Equation 1)

where $\overline{\sigma}$ is the equivalent tensile stress, Y_{SE} is the static yield strength of the sulfide glass electrolyte material, D is a reference strain rate, and n is a strain-rate-hardening



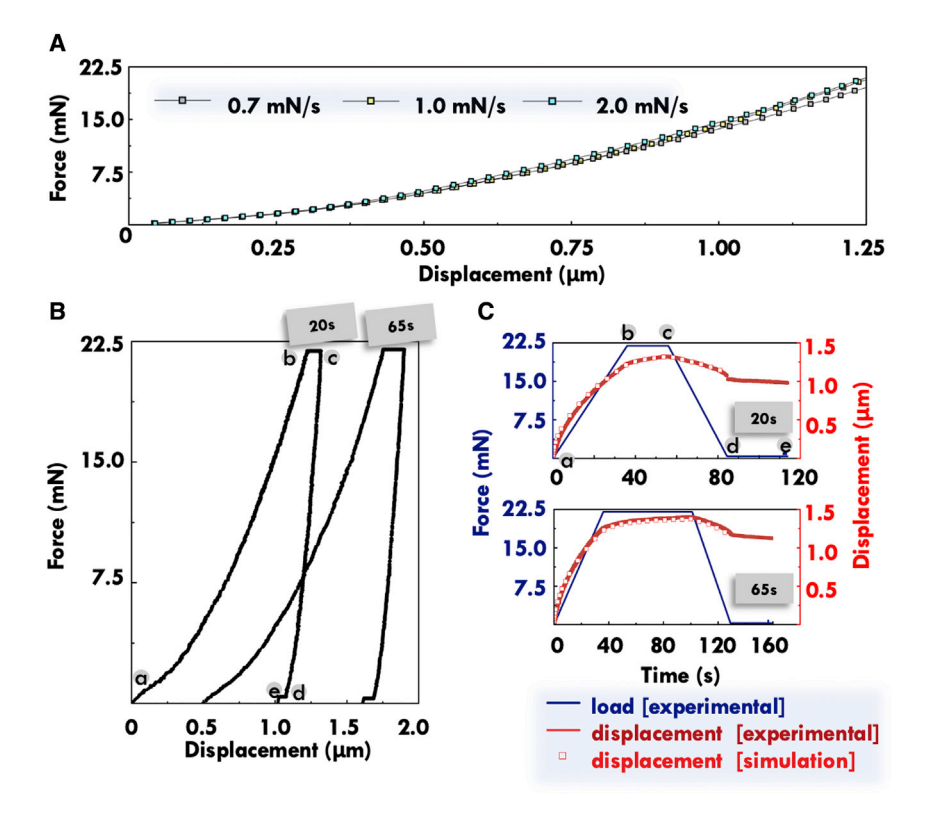


Figure 3. Nanoindentation experiments for extracting elastic modulus and time-dependent mechanical response

(A) Load-displacement curves for different loading rates of 0.7 mN/s, 1.0 mN/s, and 2.0 mN/s. (B) Load-displacement curves in the case of modified loading patterns. The measurements shown were performed with a loading rate of 1.0 mN/s (segment a–b) and an unloading rate of -1.0 mN/s (segment c–d).

(C) Viscoplastic model was fit to the experimental data for the case of 20 s holding time. The simulated load-displacement curve agreed well with the experimental data for the case of $65 \, \text{s}$.

parameter. These material parameters (Table 1) can be determined by fitting the model to the Berkovich indentation data (Figure 3C; more details in experimental procedures). Note that detailed understanding of the plastic deformation mechanism is still unclear and requires further investigation.

The sulfide glass electrolyte exhibits relatively low Young's modulus ($E_{\rm SE}=10$ GPa) and static yield strength ($Y_{\rm SE}=200$ MPa). As shown in Figure 4, these two values are much smaller than $E_{\rm SE}$ and $Y_{\rm SE}$ for crystalline oxide and sulfide electrolytes and only slightly larger than the upper-bound values for Li metal (reported Young's modulus of polycrystalline Li, $E_{\rm Li}$, ranges from ~5 to ~8 GPa and the yield strength, $Y_{\rm Li}$, ranges from ~0.1 MPa to ~100 MPa). $^{26-33}$ It is worth mentioning that the large variation in the mechanical properties of lithium is attributed to intrinsic size effects and its viscoplastic nature. $^{26-33}$ A previous nanoindentation study of LPS glass also reports an $E_{\rm SE}$ value that is lower than the polycrystalline moduli in Figure 4; however, the value in Table 1 is roughly 40% below this previous result. 15 These materials also exhibited the type of time-dependent displacement at a fixed load seen in Figure 3B (evidence of viscoplasticity), although this behavior was not directly studied in this prior work. 15,34,35 The Li₂S content of this material was the same as that used in both materials tested in the current investigation; thus, the difference is apparently due to other factors associated with the synthesis process that are difficult to discern



Table 1. Sulfide properties				
Young's modulus E (GPa)	Poisson's ratio ν	Y _{SE} (GPa)	D	n
10	0.30	0.20	0.0008	4

here, given the limited range of materials that have been studied. However, it appears that E_{SE} for these glassy materials is somewhat smaller than those recently reported for polycrystalline sulfide electrolytes (with different compositions). ³⁶

The viscoplastic deformation is also a distinctive feature of these sulfide glass electrolytes. In polycrystalline oxide and sulfide electrolytes, rate-dependent creep requires much higher loads, with yield stresses that are more than one order of magnitude higher than those measured for the sulfide glass. The operative creep mechanisms in the glass are thus likely to differ substantially from those occurring in the polycrystalline materials. Deeper understanding of these phenomena will require additional detailed characterization and modeling. However, the measurements reported here clearly indicate that, in comparison with other solid electrolyte materials, the amorphous structure and unusual viscoplastic behavior of sulfide glasses will cause these materials to respond very differently to mechanical forces. Furthermore, the constitutive law in Equation (1) makes it possible to assess the impact that this viscoplasticity will have on important phenomena during battery operation. Two relevant examples are discussed in detail in the following subsections.

Interfacial contact between the sulfide glass electrolyte and lithium metal electrode

A mechanically stable interface between the electrolyte and electrode is important for the performance and cycle life of SSBs. Monroe and Newman analyzed the interfacial stability by treating the electrolyte and Li-metal electrode as linear elastic solids and suggested that a stiff electrolyte can inhibit amplification of surface roughness (and hence dendritic growth) of the Li electrode during the plating process. These effects imply that the Monroe-Newman stability criteria must be modified for stiff ceramic electrolytes like Li lanthanum zirconium oxide (LLZO) (i.e., where the modulus far exceeds the Monroe-Newman limit). For the sulfide glasses, the lower modulus (close to Li metal) and viscoplasticity introduce additional complexity. The low yield stress suggests that sulfide electrolyte materials might deform plastically when interacting with Li electrodes and also raises concerns about whether the electrolyte is stiff enough to suppress interfacial roughening.

The analysis presented here emphasizes the impact of plasticity in the electrolyte, effects that are not included in previous analyses of electrolyte deformation. To evaluate this, a FEM model of elastoplastic contact between the sulfide glass electrolyte and Li-metal electrode was formulated. The former had a flat surface while the latter featured a two-dimensional periodic surface roughness profile, as shown in Figure 5A (more details are in experimental procedures). This model provides a qualitative understanding of the evolution of the interface under stack pressure. Significant plastic deformation was observed in both materials when upper-bound properties of lithium were employed, i.e., $E_{\rm Li}=8$ GPa and $Y_{\rm Li}=100$ MPa (Figure 5B). $^{26-33}$ The surface roughness of the Li-metal electrode was mechanically flattened by the impression of the sulfide electrolyte, and conformal interfacial contact was achieved under a stack pressure of larger than $5Y_{\rm Li}$ for a practical range of



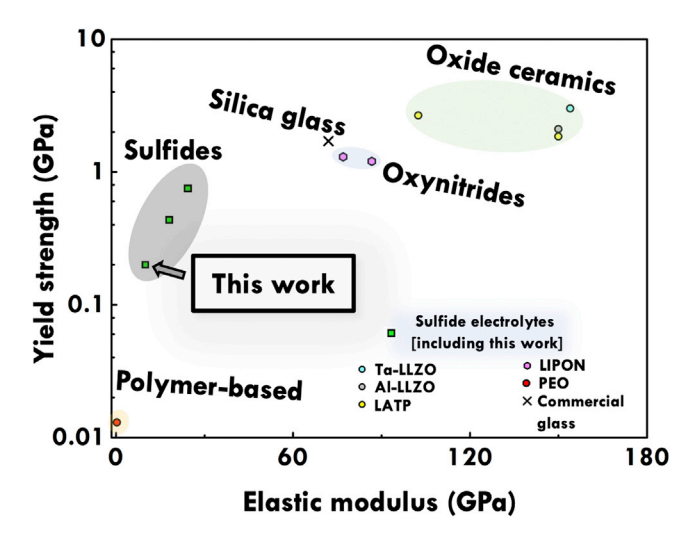


Figure 4. Ashby plot showing the yield strength and elastic modulus for various types of electrolyte materials

Colored shaded regions in the plot represent the material family charts (e.g., oxides, oxynitrides, and polymers).

roughness amplitudes and Li-metal yield strength (Figures 5B and 5C). It is expected that the ability to flatten Li electrodes can be compromised when Y_{SE} is smaller than Y_{Li} . This condition is not likely to occur with the materials tested here.

Viscoplastic effects on dendritic cracking of the sulfide glass electrolyte

While a flat sulfide glass electrolyte can suppress the amplification of surface roughening of a Li-metal electrode during plating, there are inevitably crack-like flaws and other defects on the electrolyte surface. ^{31,40,41} Li insertion into these features exerts pressure on the flaw walls. This can build up during the plating process, and at sufficiently high levels, the strain energy in the solid electrolyte can provide a driving force for the extension of the surface flaws via a fracture-like process. This is believed to be a major cause of dendrite cracking. ^{31,40,41} Previous assessment of this phenomenon assumes that the solid electrolyte is an elastic solid with high modulus, which is valid for LLZO and other oxides. However, the sulfide glass electrolyte is clearly prone to plastic deformation due to its low yield strength. There is currently very little understanding of how this plasticity, especially viscoplasticity, affects the Li penetration mechanism.

Here, we consider a pre-existing blunted crack in the sulfide glass electrolyte adjacent to the Li electrode and restrict the analysis to a two-dimensional plane strain condition (Figure 6). For simplicity, the crack is assumed to be fully infiltrated by Li, although there is also some experimental evidence showing partially filled cracks. ^{41,45} The pressure, p, on the walls exerted by Li was assumed to be uniform, under the premise that the small value of Y_{Li} leads to fluid-like behavior. ^{29,30} To obtain basic insights into the effects of viscoplastic dissipation, the accumulation of pressure was assumed to follow a linear function of time, i.e., $p = p(t) = \dot{p}t$. An energy balance is then formulated,

$$G_{\text{tip}} = G_{\text{global}} - G_{\text{plastic}}$$
 (Equation 2)

where G_{tip} is the local energy driving force at the crack tip, G_{global} is the total energy inflow due to Li pressure accumulation, and G_{plastic} is the energy dissipation

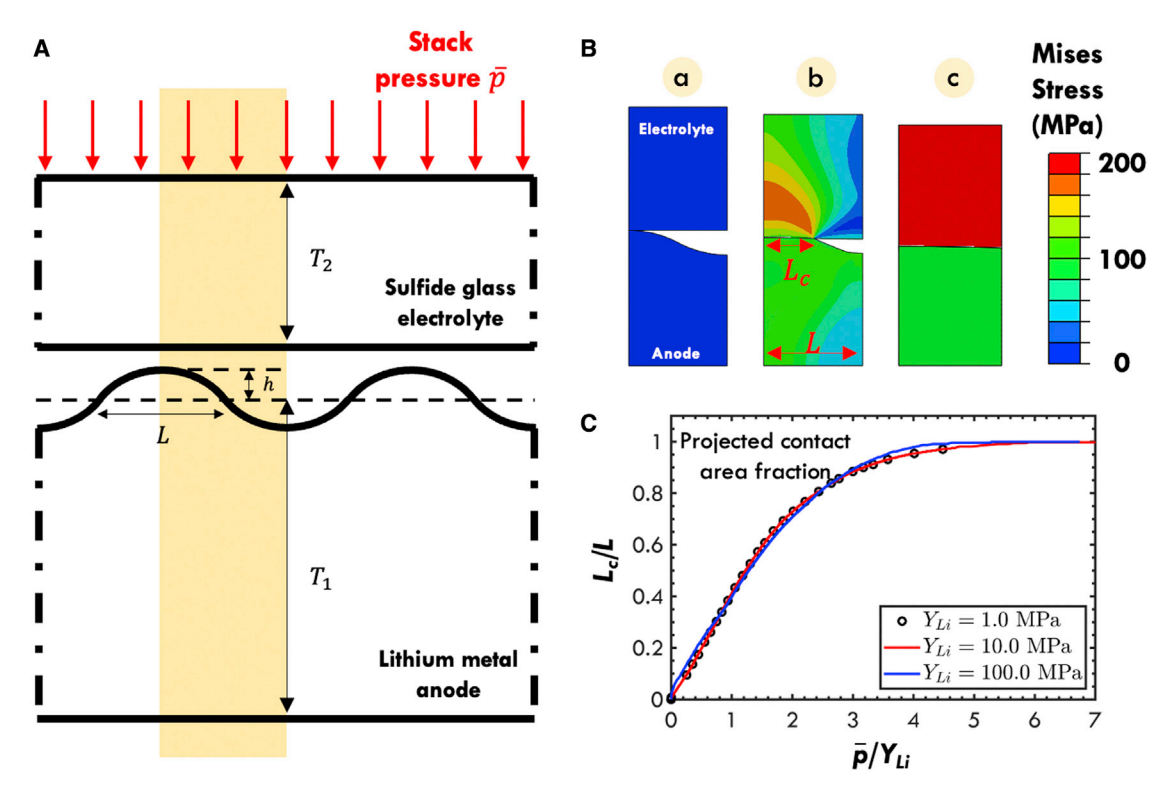


Figure 5. Mechanical contact between lithium metal electrode and the sulfide glass electrolyte

(A) The lithium electrode and the sulfide glass electrolyte were both modeled as blocks with thickness T_1 and T_2 , respectively. The electrolyte was bounded by a flat-top surface while the electrode featured a two-dimensional periodic surface roughness profile. Considering the periodicity and symmetry of the geometry, only the shaded part was modeled. A frictionless contact between the electrolyte and lithium electrode was assumed. A quasi-static displacement-controlled load was applied to the top surface of the electrolyte.

(B) The surface roughness of the lithium metal electrode was flattened by the impression of the sulfide electrolyte. Significant plastic deformation was observed in the electrolyte when $E_{Li} = 8$ GPa and $Y_{Li} = 100$ MPa.

(C) With a small roughness amplitude of $h/L = \frac{1}{8}$, a conformal interfacial contact was achieved under a stack pressurelarger than $5Y_{Li}$.

associated with viscoplastic flow around the crack tip. Note that the crack extension is initiated when G_{tip} exceeds the intrinsic fracture resistance (e.g., surface energies) of the electrolyte, G_c , and we assume that the mechanical behavior of the electrolyte near the crack tip is still governed by the calibrated viscoplasticity model in simulation-assisted Berkovich indentation. 46 Results obtained for a selected length $I_{\rm c}$ = 10.0 μ m and tip radius ρ = 0.1 μ m (Figure 6) show that $G_{\rm tip}$ exhibits a strong dependence on the instantaneous pressure, p, and its accumulation rate, \dot{p} (more details in experimental procedures). In other words, when the same instantaneous pressure is reached with different loading rates, \dot{p} , there are substantial differences in $G_{\rm tip}$. With large \dot{p} values, the sulfide glass material does not have enough time to dissipate energy through viscoplastic deformation and a larger driving force builds up in the crack tip. This suggests that dendrite propagation due to electrolyte fracture will be initiated more readily at a lower instantaneous pressure under conditions where the loading rate (i.e., current density) is higher. This model does not yet include a full description of Li plating and deformation; however, it provides a qualitative understanding of the impact of electrolyte viscoplasticity on dendrite growth, i.e., showing that fast pressure buildup makes the sulfide glass electrolyte more prone to Li penetration.

Intuitively, pressure buildup inside surface flaws is associated with the lithium flux during plating, as well as the viscoplastic deformation of the Li. These processes



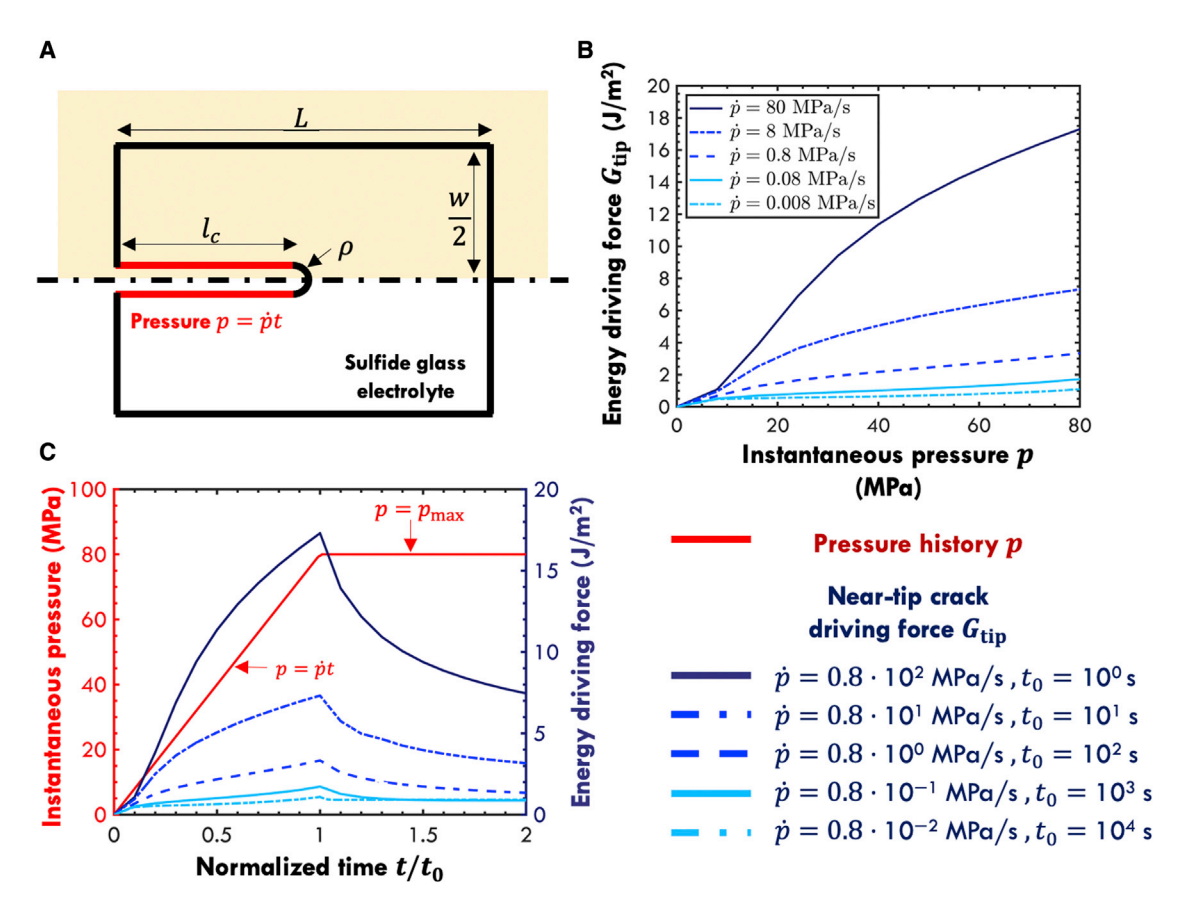


Figure 6. Viscoplastic effects on dendritic cracking of the sulfide glass electrolyte

(A) A two-dimensional block (of length $L=30~\mu m$ and width $w=20~\mu m$) of the sulfide glass material with blunted crack (of length $l_c=10~\mu m$ and tip radius $\rho=0.1~\mu m$) was modeled. A uniform pressure p was exerted on the crack walls. By utilizing the symmetry of the model, only the top half was modeled (shaded in yellow). Domain J integrals were performed at the crack tip to evaluate the local energy driving force $G_{\rm tip}$.

(B) G_{tip} showed a strong dependence on the instantaneous pressure, p, and its accumulation rate, \dot{p} . Faster pressure buildup (i.e., larger \dot{p}) leads to a larger value of G_{tip} at the point where a given pressure is reached.

(C) The evolution of local energy driving force exhibits a strong dependence on the pressure accumulation rates.

will be a strong function of the charging current density, i_o . This relationship will depend on several interrelated phenomena, including the size of the surface flaw, the pressure-driven flow of Li, and the properties of the electrolyte. A full model of these processes is beyond the scope of the treatment presented here. While several recent models have addressed some aspects of this, there is very little direct information about the key mechanisms occurring at these length scales, and thus, a reliable relationship between the pressure buildup and the current density is not available. 29,30,39,47 Simplified models predict that pressure is proportional to i_0 ; however, at higher values, the pressure buildup will counteract the thermodynamic driving force for plating and thus lead to an upper-bound limit on the pressure. 29,30,39,47 In light of the complex relationship between p(t) and i_o , it is more straightforward to address the impact of viscoplasticity by considering the impact of pressure directly. The baseline for this assessment is a fully elastic electrolyte where G_{tip} is proportional to p^2 . With a viscoplastic electrolyte, this elastic limit will be approached at high rates, but at slower rates, plasticity can substantially decrease G_{tip} . The results in Figure 6B illustrate this effect and show that viscoplasticity in the electrolyte can potentially mitigate the likelihood of fracture (i.e., the



value of G_{tip}). This indicates that viscoplasticity is potentially an important factor that can impact fast charging with sulfide glass electrolytes.

Potential advantages of viscoplastic solid electrolytes

The deformation observed in sulfide glasses suggests that these materials are amenable to strategies for mitigating dendrite propagation, in ways that are not accessible in LLZO and other oxide solid electrolytes. An important effect here is that cycling at a current that is below the critical current density (CCD) should reduce G_{tip} by inducing plastic deformation of the sulfide in the vicinity of pressurized flaws. The implications of this effect are illustrated in Figure 6C, where the results correspond to cases where the pressure in a Li-filled flaw increases at different rates, up to a fixed steady-state stress of 80 MPa. This value is large enough to fracture a low toughness brittle electrolyte (if the surface flaw is large enough);³⁹ however, this process is not directly analyzed with the current model. Note that hydrostatic stress that greatly exceeds the yield stress is possible in a confined region (i.e., the tip of narrow flaw), with plasticity leading to lower stresses near the base of the flaw. The current description also neglects other factors that should ultimately be added to provide a full description. Key effects that have been treated elsewhere include current focusing at the tip of the Li protrusion³⁰ and the reduced thermodynamic driving force for plating due to the elastic energy in the Li metal (i.e., electrochemo-mechanical coupling).3

The energy release rate analysis here is substantially different from other recent models that treat the electrolyte as a simple elastic solid.^{29,47} Incorporating the experimentally verified description in Equation (1) makes it possible to obtain a physically realistic description of rate-dependent deformation in the electrolyte, something which was not feasible in previous modeling efforts. The results in Figure 6 are also based on the premise that, at a constant i_0 and with pressures that are not large enough to induce solid electrolyte fracture, there is a steady-state stress field inside of the flaw where the Li flux into the flaw (at the tip and along the sides) is balanced by Li flow out of the base of the tip. For simplicity, a uniform pressure in the filament was used for these calculations (this is a reasonable approximation if Li loss out of the base of the filament is negligible). A flaw with the dimensions shown in Figure 6A is used to illustrate the role of rate-dependent deformation in the solid electrolyte. The wider range of flaw dimensions that exist in real materials will lead to quantitative differences, but the example shown here is sufficient to illustrate the key effects. For the 80-MPa final stress in Figure 6C, a moderately high pressure accumulation rate of \dot{p} = 8 MPa/s leads to a $G_{\rm tip}$ = \sim 7 J/m² after 10 s. For a fully elastic solid electrolyte with the same modulus as the sulfide glass, $G_{\rm tip}\gg 17~{\rm J/m^2}$ (independent of time). This comparison illustrates the way in which viscoplastic creep can mitigate fracture and Li penetration (i.e., the substantially higher G_{tip} for the fully elastic case indicates that fracture occurs more readily).

Pressure increases in a static flaw will generally correspond to transients that occur as the current increases. With this in mind, the results in Figure 6C can be interpreted as scenarios where the current increases at different rates, up to a final i_0 value that results in the steady-state Li pressure of 80 MPa. Viscoplasticity in the solid electrolyte then leads to faster increases in $G_{\rm tip}$ when the current increases at a faster rate. This differs from a fully elastic electrolyte, where $G_{\rm tip}$ has the fixed, rate-independent value described above. If the pressure (or the current) increase occurs at the higher \dot{p} values in Figure 6C, then $G_{\rm tip}$ still exceeds the fracture limit. However, if the current increase occurs more slowly, viscoplastic creep in the solid electrolyte leads to a substantially lower $G_{\rm tip}$ value, such that fracture should not occur. In all cases,

Article



viscoplasticity also leads to a relaxation in $G_{\rm tip}$ at the final fixed pressure. This is due solely to creep in the solid electrolyte that leads to permanent deformation around the Li-filled flaw. This example demonstrates an important difference between sulfide electrolytes and ceramic oxides and suggests that control of viscoplastic deformation can improve resistance to Li metal penetration.

The steady-state case with uniform pressure inside of the flaw is an idealized case that illustrates the impact that viscoplasticity can have on decreasing G_{tip} . This configuration corresponds to the limiting case considered in some previous work, where Li flow out of the flaw is negligible and the steady-state pressure reaches the thermodynamic limit (an upper bound) where the strain energy in the Li counteracts the electrochemical driving force and prevents additional flow into the flaw.²⁹ Several models of the complex processes that occur during plating in a surface flaw have also been developed, but they rely on a variety of unverified assumptions, and thus incorporating viscoplasticity into these frameworks does not provide much additional insight at this time. 30,47 In general, Li flow out of the base of the flaw can potentially produce a pressure gradient along the flaw, and this should decrease G_{tip} . The idea that stresses in the flaw (especially near the tip) will induce creep in the electrolyte and mitigate fracture is still valid. Cycling protocols that enable this localized creep of the solid electrolyte before fracture occurs have the potential to suppress Li penetration. The basic dendritic cracking model presented here indicates that the fracture-like propagation of dendrites in sulfide glasses is likely to be rate dependent, with failure occurring more readily for fast pressure buildup. More specifically, the driving force for cracking depends on both the instantaneous pressure and the pressure accumulation rate. The model predicts that rapid or instantaneous changes in the current density are likely to create a larger pressure buildup inside of pre-existing cracks. These pressures should then decrease under galvanostatic conditions, as seen in Figure 6C. This implies that plating at relatively high current densities can be enabled, as long as maximum pressure values are below the threshold for the extension of pressurized Li filaments. Creep of the solid electrolyte under galvanostatic conditions should then alter the flaw shape in ways that decrease G_{tip} and thus increase the current threshold where dendrite propagation is initiated.

In summary, the rate-dependent mechanical properties of sulfide glass electrolytes were investigated. The viscous behavior was characterized with a nanoindentation creep test as follows: (1) loading at a rate of $\sim\!1.0$ mN/s, (2) holding at the maximum load, (3) unloading to a fix load of approximately 5% of the maximum value, and (4) holding at this preset lower force for a time that exceeds the duration used at the maximum load. This methodology shows that the material is primarily viscoplastic (rather than viscoelastic) at the experimental timescales. Measurements that account for this rate-dependent deformation give an elastic modulus of $\sim\!10$ GPa, along with a static yield strength of 0.2 GPa. The plasticity observed in these materials demonstrates that the deformation of these sulfide glasses differs considerably from the behavior of polycrystalline oxide and sulfide electrolytes. The observed impact of strain rates also means that the fracture toughness value of $\sim\!0.25$ MPa m $^{1/2}$ obtained from standard indentation methods based on previous work 15 is not a general material property and thus provides only approximate information about the fracture resistance.

The measurements reported here provide an initial understanding of sulfide electrolyte mechanical properties. This is necessary for predictive modeling of elastic stress distributions and fracture conditions in SSB structures. In particular, the viscoplastic



deformation of sulfide glasses that is documented in this study has important implications for the implementation of these materials in SSBs. The comparisons in Figure 4 show that the mechanical properties for sulfide glasses are in a different regime than other solid electrolytes. The experiments and corresponding analysis highlight challenges that are associated with properly measuring and describing the toughness of these materials. Based on the experimental results and analysis presented above, the inelastic deformation of the materials tested here is not expected to improve contact with Li-metal anodes at normal stack pressures. However, the regimes in Figure 4 suggest that modest changes in the mechanical properties might lead to conditions where viscoplasticity can improve contact. The results presented here also highlight the influence of viscoplasticity on fracture and related processes. An intriguing possibility is that viscoplastic deformation may mitigate stress-driven Li-metal penetration through the electrolyte. This is based on the premise that local inelastic deformation of the solid electrolyte will decrease local stress concentrations near the filament tip. Here, analysis of pressure buildup in a surface flaw indicates that the fracture-like propagation of dendrites in sulfide glasses is likely to be rate dependent, with failure occurring more readily at higher charge rates.

EXPERIMENTAL PROCEDURES

Resource availability

Lead contact

Further information and requests for resources should be directed to and will be fulfilled by the lead contact, Christos E. Athanasiou (christos_edouardos_athanasiou@brown.edu).

Materials availability

The sulfide electrolyte materials were provided by Polyplus Battery Company.

Data and code availability

All data and code associated with the study are available from the lead contact upon reasonable request.

Sample preparation

The sulfide electrolytes were prepared by melt quenching. Li sulfide (the network modifier) was mixed with a network former (P₂S₅, B₂S₃, and SiS₂), where the ratio of network modifier to network former was 7:3 (mole ratio). Raw-material powders were weighed and mixed in a glovebox (<1 ppm H₂O and O₂) and loaded into a non-reactive crucible (vitreous carbon, boron nitride, and silicon nitride), and the crucible was loaded into a quartz ampoule. The contents were sealed under vacuum using a hydrogen/oxygen torch, placed into a rocking furnace, heated to ≥900°C for an hour or more, and then quenched in water and annealed to yield a solid ingot of glass with high ionic conductivity (7 \times 10⁻⁴ S/cm at room temperature). This meltquenching process produced glass that is completely amorphous, with no detectable porosity. These materials are significantly more homogeneous than other sulfide electrolytes produced from pressed powders, which typically contain significant porosity. 36,48 The flat, disc-like samples (shown at the inset of Figures 1B and 1C) were ~28 mm in diameter, ~2 mm thick, and weighed 2.02 g. They were polished with fine-grit sandpaper. After processing, the samples were kept in plastic boxes in heat-sealed plastic-metal pouches inside an Ar-filled glove box. To eliminate contamination during transferring (i.e., due to the vacuum cycles in the glove box antechamber), a specialized vacuum can was assembled (Figure S1). The degradation of sulfide glasses in the presence of moisture was accompanied with a change in coloration and morphology. Thus, all the processing and mounting steps were

Article



conducted inside an Ar-filled glovebox with less than 10 ppm H_2O and 1 ppm O_2 . The mechanical testing was performed in a liquid cell filled with mineral oil. Based on Figure S2, all the samples were tested within 1 h and did not exhibit any visible changes in color or opacity throughout the experiments. ^{15,34}

Instrumented Berkovich indentation

To investigate the elastic and plastic behaviors of the sulfide glass materials via instrumented Berkovich indentation (Hysitron TI 900, MN, USA), flat and polished samples were mounted within a specialized fluid cell as shown in Figure 1, which was filled with mineral oil (Alfa Aesar, MA, USA). The indenter tip was immersed fully in the liquid medium during testing. 15 The sample was covered by a shallow mineral film of $\sim\!0.5$ mm to eliminate potential impact of buoyancy effects on the indentation load measurements. The instruments' frame compliance was carefully calibrated using a series of depth measurements on reference fused silica materials. The measurements were collected at five distinct sample surface locations with center-to-center spacing of more than 150 μm . The maximum indentation depth was $\sim\!\!2~\mu m$ and thus much less than the 2 mm sample thickness. Thus, finite-thickness effects were reasonably neglected. 17 The loading pattern for the tests shown in Figures 1B and 1C was loading up to 20 mN with 1 mN/s and then unloading with a 1 mN/s rate.

Vickers indentation fracture

To investigate the fracture responses of the sulfide glass materials, Vickers indentation (ZHV10, Zwick, Germany) was used. Again, the sample was submerged in mineral oil while placed in a 35-mm-diameter Petri dish. The indentation loading time was fixed at 30 s (Figure 2A) and holding steps of 15, 30, 60, 300, and 1,000 s (see dashed lines in Figure 2A). After indentation, the liquid cell was transferred to the optical microscope for measuring the crack length with the $50\times$ objective. All the patterns were imaged in dark field to provide the best contrast for measuring crack length of the immersed sulfide glasses in the oil. Each data point shown in Figure 2C is an average of three measurements. Based on the previously measured hardness and elastic modulus values, the estimates of an apparent $K_{\rm IC}$ for different holding times and applied maximum loads were obtained by the Anstis et al.²⁰ relation

$$K_{\rm IC} = k \left(\frac{E}{H}\right)^{1/2} \left(\frac{F}{c^{3/2}}\right)$$
 (Equation 3)

where c is the measured crack length, E is the elastic modulus, H is the hardness, and k is 0.016 for the Vickers geometry.

Study of creep using instrumented Berkovich indentation

The setup used was the same as that described for the aforementioned instrumented Berkovich indentation method. Two types of load-controlled indentation measurements shown in Figures 3B and 3C were performed with a loading rate of 1 mN/s. The loading pattern is shown in Figure 3C (blue line). The unloading rate was 1 mN/s. The holding time was 20 and 65 s.

Finite element modeling of mechanical contact between lithium and the sulfide glass electrolyte

FEM simulations were performed to predict the response of a rough surface of Limetal electrode when it was mechanically impressed by the sulfide glass electrolyte. Both the Li electrode and the sulfide glass electrolyte were modeled as blocks with thickness T_1 and T_2 , respectively (Figure 5A). The electrolyte had a flat-top surface,



while the electrode featured a rough surface. The surface roughness of the electrode was idealized as a two-dimensional periodic profile, consisting of concave and convex arcs with chord length L and sagitta h (Figure 5A). The roughness amplitude h was significantly smaller than the thickness of each plate ($h \le 0.05T_{1,2}$), which eliminated the effects of the bottom boundary and approximated two semi-infinite solids. By utilizing the periodicity and symmetry of the surface roughness, a twodimensional reduced model was formulated (shaded in yellow in Figure 5A) with the plane strain assumption in Abaqus. 49 An encastré boundary condition was applied to the bottom surface of the lithium electrode and a displacementcontrolled boundary condition to the top surface of the electrolyte. Horizontal displacements were constrained on the planes of symmetry in both parts. The contact between the electrolyte and Li electrode was assumed frictionless. Both parts were meshed with more than 100,000 full integration elements (CPE3 and CPE4). A quasistatic displacement-controlled load was applied to the top surface of the electrolyte part. Therefore, any rate-dependent material effects can be ignored, and both the sulfide glass electrolyte and Li metal were modeled as elastic-perfectly-plastic material with different elastic constants and yield strengths (E_{SE} = 10 GPa, ν_{SE} = 0.3, Y_{SE} = 200 MPa, E_{Li} = 8 GPa, ν_{Li} = 0.3, and Y_{Li} = 1–100 MPa). The morphology of the contact region was monitored (Figure 5B), as well as the projected contact area and stack pressure (Figure 5C). Note that, in most cases, the roughness amplitude h is significantly less than the wavelength L. In our simulations, the ratio was fixed as $h/L = \frac{1}{8}$.

Evaluation of the driving force for dendritic cracking

A two-dimensional block (of length $L=30.0~\mu m$ and width $w=20.0~\mu m$) of the sulfide glass electrolyte with a blunted surface crack was considered. The blunted crack had a length of $I_c=10.0~\mu m$ and a tip radius of $\rho=0.1~\mu m$ (Figure 6). A plane strain condition was employed. A uniform pressure p was exerted on the crack walls, which followed a linear function of time, i.e., $p=p(t)=\dot{p}t$. By utilizing the symmetry of the model, only the top half was modeled (shaded in yellow in Figure 6A). The viscoplasticity constitutive model for the sulfide glass material was implemented through a user-defined subroutine (UMAT) in Abaqus (Table 1). Symmetric boundary conditions were applied to the right and bottom surfaces of the ½ model. Domain J-integral calculations were performed at different positions from the crack tip. More than 100,000 two-dimensional reduced integration elements (CPE8R) were employed with refined mesh near the crack tip. The J integral at the tip provided the local energy driving force $G_{\rm tip}$. A saturated J integral was obtained as the integral contour enclosed the yielding zone, which gave the global energy inflow by Li pressure accumulation, $G_{\rm global}$.

Finite element modeling of Berkovich indentation

FEM simulations were performed to understand the load-displacement response of the sulfide glass sample when it was impressed by a Berkovich pyramidal indenter (with a centerline-to-face angle of 65.3°). The sulfide glass electrolyte was described by a large-deformation elastic-viscoplasticity constitutive model with the Peirce formulation, while the indenter was assumed to be rigid. The viscoplasticity model was implemented through a user-defined subroutine (UMAT) in Abaqus. ⁴⁹ The sulfide glass bulk sample was modeled as a cylinder (Figure 7) with radius $R=20.0~\mu m$ and height $H=10.0~\mu m$, both of which were much larger than the imprint size of the indentation ($\sim 1~\mu m$) to eliminate the effects of boundaries. The cylinder model was further simplified to a 6-fold symmetric model (1/6 cylinder in Figure 7) by utilizing the symmetry of the Berkovich indenter. Symmetric boundary conditions were applied to the 6-fold symmetry planes of the cylinder and an encastré boundary



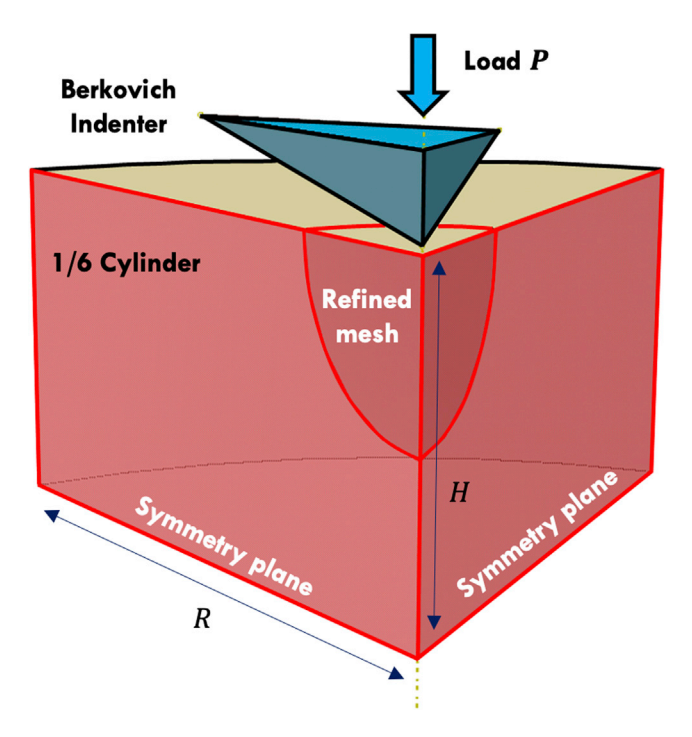


Figure 7. Finite element modeling of Berkovich indentation of the sulfide glass bulk sample

The sulfide glass bulk sample was modeled as a cylinder with radius *R* and height *H*. By utilizing the symmetry of the Berkovich indenter, the model was simplified to a 1/6 cylinder to reduce the computational cost. Symmetric boundary conditions were applied to the 6-fold symmetry planes of the cylinder and an encastré boundary condition to the bottom surface. A frictionless contact between the top surface of the cylinder and the indenter was assumed in the simulation. A time-dependent load was applied to the indenter while the indentation displacement is recorded over time.

condition to the bottom surface (Figure 7). The contact between the top surface of the cylinder and the indenter was assumed frictionless. More than 100,000 three-dimensional full integration elements (C3D6 and C3D8) were employed with refined mesh near the contact region (Figure 7). A time-dependent load (as shown in Figure 3C) was applied to the indenter, and the history of indentation displacement was recorded during the simulation.

SUPPLEMENTAL INFORMATION

Supplemental information can be found online at https://doi.org/10.1016/j.xcrp. 2022.100845.

ACKNOWLEDGMENTS

The authors acknowledge financial support from SK Innovation and the National Science Foundation (DMR-2124775).

AUTHOR CONTRIBUTIONS

C.E.A., X.L., and B.W.S. planned the project with the help of C.L., M.P., J.Y., N.P.P., and H.G. C.E.A. and X.L. performed the experiments and simulations with the help of M.Y.J., E.N., and S.V. The manuscript was written by C.E.A., X.L., and B.W.S. and revised by N.P.P. and H.G. All authors contributed to discussions and analysis.



Cell Reports Physical Science Article

DECLARATION OF INTERESTS

The authors declare no competing interests.

Received: January 4, 2022 Revised: February 17, 2022 Accepted: March 16, 2022 Published: April 6, 2022

REFERENCES

- Albertus, P., Anandan, V., Ban, C., Balsara, N., Belharouak, I., Buettner-Garrett, J., Chen, Z., Daniel, C., Doeff, M., Dudney, N.J., et al. (2021). Challenges for and pathways toward Li-Metal-Based all-solid-state batteries. ACS Energy Lett. 4, 1399–1404.
- Hatzell, K.B., Chen, X.C., Cobb, C.L., Dasgupta, N.P., Dixit, M.B., Marbella, L.E., McDowell, M.T., Mukherjee, P.P., Verma, A., Viswanathan, V., et al. (2020). Challenges in lithium metal anodes for solid-state batteries. ACS Energy Lett. 5, 922–934.
- Kim, K.J., Balaish, M., Wadaguchi, M., Kong, L., and Rupp, J.L.M. (2021). Solid-state Li-metal batteries: challenges and horizons of oxide and sulfide solid electrolytes and their interfaces. Adv. Energy Mater. 11, 2002689.
- Kazyak, E., Garcia-Mendez, R., LePage, W.S., Sharafi, A., Davis, A.L., Sanchez, A.J., Chen, K.-H., Haslam, C., Sakamoto, J., and Dasgupta, N.P. (2020). Li penetration in ceramic solid electrolytes: operando microscopy analysis of morphology, propagation, and reversibility. Matter 2, 1025–1048.
- 5. Takada, K. (2013). Progress and prospective of solid-state lithium batteries. Acta Mater. 61,
- Mercier, R., Malugani, J.P., Fahys, B., and Robert, G. (1981). Superionic conduction in Li₂S-P₂S₅-Lil-glasses. Solid State Ion 5, 663–666.
- Pradel, A., and Ribes, M. (1986). Electrical properties of lithium conductive silicon sulfide glasses prepared by twin roller quenching. Solid State Ion 18–19, 351–355.
- Minami, K., Mizuno, F., Hayashi, A., and Tatsumisago, M. (2007). Lithium ion conductivity of the Li2S-P2S5 glass-based electrolytes prepared by the melt quenching method. Solid State Ion 178, 837–841.
- Li, J., Ma, C., Chi, M., Liang, C., and Dudney, N.J. (2015). Solid electrolyte: the key for highvoltage lithium batteries. Adv. Energy Mater. 5, 1401408.
- Kudu, Ö.U., Famprikis, T., Fleutot, B., Braida, M.-D., Le Mercier, T., Islam, M.S., and Masquelier, C. (2018). A review of structural properties and synthesis methods of solid electrolyte materials in the Li2S – P2S5 binary system. J. Power Sourc. 407, 31–43.
- Liu, Z., Fu, W., Payzant, E.A., Yu, X., Wu, Z., Dudney, N.J., Kiggans, J., Hong, K., Rondinone, A.J., and Liang, C. (2013). Anomalous high ionic conductivity of nanoporous β-Li₃-PS₄. J. Am. Chem. Soc. *135*, 975–978.

- Seino, Y., Ota, T., Takada, K., Hayashi, A., and Tatsumisago, M. (2014). A sulfide lithium super ion conductor is superior to liquid ion conductors for use in rechargeable batteries. Energy Environ. Sci 7, 627–631.
- 13. Kamaya, N., Homma, K., Yamakawa, Y., Hirayama, M., Kanno, R., Yonemura, M., Kamiyama, T., Kato, Y., Hama, S., Kawamoto, K., et al. (2011). A lithium superionic conductor. Nat. Mater. 10, 682–686.
- Bishop, S.R., Marrocchelli, D., Chatzichristodoulou, C., Perry, N.H., Mogensen, M.B., Tuller, H.L., and Wachsman, E.D. (2014). Chemical Expansion: implications for electrochemical energy storage and conversion devices. Annu. Rev. Mater. Res. 44, 205–239
- McGrogan, F.P., Swamy, T., Bishop, S.R., Eggleton, E., Porz, L., Chen, X., Chiang, Y., and Van Vliet, K.J. (2017). Compliant yet brittle mechanical behavior of Li₂S-P₂S₅ lithium-ionconducting solid electrolyte. Adv. Energy Mater. 7, 1602011.
- Hysitron. (2014). TI 950 TriboIndenter User Manual (Hysitron Incorporated).
- 17. Fischer-Cripps, A.C. (2011). Nanoidentation (Springer-Verlag).
- Oliver, W.C., and Pharr, G.M. (1992). An improved technique for determining hardness and elastic modulus using load and displacement sensing indentation experiments. J. Mater. Res. 7, 1564–1583.
- Oliver, W.C., and Pharr, G.M. (2004). Measurement of hardness and elastic modulus by instrumented indentation: advances in understanding and refinements to methodology. J. Mater. Res. 19, 18.
- Anstis, G.R., Chantikul, P., Lawn, B.R., and Marshall, D.B. (1981). A critical evaluation of indentation techniques for measuring fracture toughness: I, direct crack measurements. J. Am. Ceram. Soc. 64, 533–538.
- Athanasiou, C.-E., and Bellouard, Y. (2015). A monolithic micro-tensile tester for investigating silicon dioxide polymorph micromechanics, fabricated and operated using a femtosecond laser. Micromachines 6, 1365–1386.
- Liu, X., Athanasiou, C.E., Padture, N.P., Sheldon, B.W., and Gao, H. (2020). A machine learning approach to fracture mechanics problems. Acta Mater. 190, 105–112.
- Liu, X., Athanasiou, C.E., Padture, N.P., Sheldon, B.W., and Gao, H. (2021). Knowledge extraction and transfer in data-driven fracture

- mechanics. Proc. Natl. Acad. Sci. U S A *118*, e2104765118.
- Yang, S., Zhang, Y.-W., and Zeng, K. (2004). Analysis of nanoindentation creep for polymeric materials. J. Appl. Phys. 95, 3655– 3666.
- Perić, D., and Owen, D.R.J. (1992). A model for large deformations of elasto-viscoplastic solids at finite strain: computational issues. In Finite Inelastic Deformations—Theory and Applications (Springer), pp. 299–312.
- Xu, C., Ahmad, Z., Aryanfar, A., Viswanathan, V., and Greer, J.R. (2017). Enhanced strength and temperature dependence of mechanical properties of Li at small scales and its implications for Li metal anodes. Proc. Natl. Acad. Sci. U S A 114. 57–61.
- Herbert, E.G., Hackney, S.A., Thole, V., Dudney, N.J., and Phani, P.S. (2018a). Nanoindentation of high-purity vapor deposited lithium films: a mechanistic rationalization of diffusion-mediated flow. J. Mater. Res. 33. 1347–1360.
- 28. Narayan, S., and Anand, L. (2018). A large deformation elastic–viscoplastic model for lithium. Extreme Mech. Lett. 24, 21–29.
- Klinsmann, M., Hildebrand, F.E., Ganser, M., and McMeeking, R.M. (2019). Dendritic cracking in solid electrolytes driven by lithium insertion. J. Power Sourc. 442, 227226.
- Barroso-Luque, L., Tu, Q., and Ceder, G. (2020). An analysis of solid-state Electrodepositioninduced metal plastic flow and predictions of stress states in solid ionic conductor defects.
 J. Electrochem. Soc. 167, 020534.
- Swamy, T., Park, R., Sheldon, B.W., Rettenwander, D., Porz, L., Berendts, S., Uecker, R., Carter, W.C., and Chiang, Y.-M. (2018). Lithium metal penetration induced by Electrodeposition through solid electrolytes: example in single-crystal Li₆La₃ZrTaO₁₂ garnet. J. Electrochem. Soc. 165, A3648–A3655.
- 32. Fincher, C.D., Ojeda, D., Zhang, Y., Pharr, G.M., and Pharr, M. (2020). Mechanical properties of metallic lithium: from nano to bulk scales. Acta Mater. 186, 215–222.
- LePage, W.S., Chen, Y., Kazyak, E., Chen, K.-H., Sanchez, A., Poli, A., Arruda, E.M., Thouless, M.D., and Dasgupta, N.P. (2019). Lithium mechanics: roles of strain rate and temperature and implications for lithium metal batteries.
 J. Electrochem. Soc. 166, A89–A97.
- 34. McGrogan, F.P. (2018). Electrochemomechanical Fatigue and Fracture

Article



- in Electrode and Electrolyte Materials for Li-Ion Batteries" (MIT), PhD Thesis.
- 35. McGrogan, F.P. (2022). SageGlass, Faribault, Minnesota, private communication.
- 36. Papakyriakou, M., Lu, M., Liu, Y., Liu, Z., Chen, H., McDowell, M.T., and Xia, S. (2021). Mechanical behavior of inorganic lithium-conducting solid electrolytes. J. Power Sourc. 516, 230672.
- 37. Monroe, C., and Newman, J. (2004). The effect of interfacial deformation on Electrodeposition kinetics. J. Electrochem. Soc. 151, A880.
- 38. Monroe, C., and Newman, J. (2005). The impact of elastic deformation on deposition kinetics at lithium/polymer interfaces. J. Electrochem. Soc. 152, A396.
- Porz, L., Swamy, T., Sheldon, B.W., Rettenwander, D., Frömling, T., Thaman, H.L., Berendts, S., Uecker, R., Carter, W.C., and Chiang, Y. (2017). Mechanism of lithium metal penetration through inorganic solid electrolytes. Adv. Energy Mater. 7, 1701003.

- Athanasiou, C.E., Jin, M.Y., Ramirez, C., Padture, N.P., and Sheldon, B.W. (2020). Hightoughness inorganic solid electrolytes via the use of reduced graphene oxide. Matter 3, 212–229.
- Ning, Z., Jolly, D.S., Li, G., De Meyere, R., Pu, S.D., Chen, Y., Kasemchainan, J., Ihli, J., Gong, C., Liu, B., et al. (2021). Visualizing platinginduced cracking in lithium-anode solidelectrolyte cells. Nat. Mater. 20, 1121–1129.
- Zhang, X., Wang, Q.J., Harrison, K.L., Roberts, S.A., and Harris, S.J. (2020). Pressure-driven interface evolution in solid-state lithium metal batteries. Cell Rep. Phys. Sci. 1, 100012.
- Krauskopf, T., Hartmann, H., Zeier, W.G., and Janek, J. (2019). Toward a fundamental understanding of the lithium metal anode in solid-state batteries—an Electrochemomechanical study on the garnet-type solid electrolyte Li_{6.25}Al_{0.25}La₃ Zr₂O₁₂. ACS Appl. Mater. Inter. 11, 14463–14477.
- 44. Doux, J.-M., Yang, Y., Tan, D.H.S., Nguyen, H., Wu, E.A., Wang, X., Banerjee, A., and Meng, Y.S. (2020). Pressure effects on sulfide

- electrolytes for all solid-state batteries. J. Mater. Chem. A. *8*, 5049–5055.
- Hao, S., Bailey, J.J., Iacoviello, F., Bu, J., Grant, P.S., Brett, D.J.L., and Shearing, P.R. (2021). 3D imaging of lithium protrusions in solid-state lithium batteries using X-ray computed tomography. Adv. Funct. Mater. 31, 2007564.
- Tvergaard, V., and Hutchinson, J.W. (1992). The relation between crack growth resistance and fracture process parameters in elastic-plastic solids. J. Mech. Phys. Sol. 40, 1377–1397.
- Shishvan, S.S., Fleck, N.A., McMeeking, R.M., and Deshpande, V.S. (2020). Dendrites as climbing dislocations in ceramic electrolytes: initiation of growth. J. Power Sourc. 456, 227989.
- Sakuda, A., Hayashi, A., and Tatsumisago, M. (2013). Sulfide solid electrolyte with favorable mechanical property for all-solid-state lithium battery. Sci. Rep. 3, 2261.
- 49. Abaqus. (2010). Abaqus Reference Manuals (Dassault Systèmes Simulia).